Submitted to Nuclear Physics A

LBL-4080
Preprint

DIFFUSION PROCESSES IN THE RELAXED CROSS SECTION FOR THE REACTION $^{107,109}Ag + ^{20}Ne$

R. Babinet, L. G. Moretto, J. Galin, R. Jared,
J. Moulton, and S. G. Thompson

August 1975

Prepared for the U. S. Energy Research and
Development Administration under Contract W-7405-ENG-48

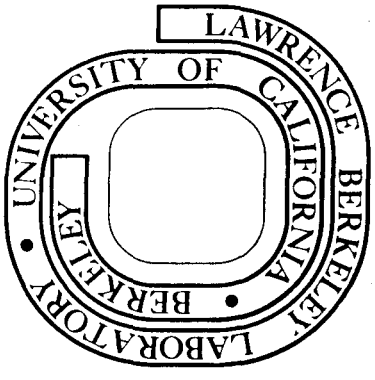

DISCLAIMER

DIFFUSION PROCESSES IN THE RELAXED CROSS SECTION FOR THE REACTION $^{107,109}Ag + ^{20}Ne$

R. Babinet,[†] L. G. Moretto,[‡] J. Galin,[*]
R. Jared, J. Moulton and S. G. Thompson

Department of Chemistry
and
Lawrence Berkeley Laboratory
University of California
Berkeley, California 94720

ABSTRACT

The fragments emitted in the reaction $^{107,109}Ag + ^{20}Ne$ at 175 MeV and 252 MeV bombarding energy have been identified in charge up to Z = 32. Kinetic energy distributions, cross sections and angular distributions have been measured for each Z. The kinetic energy spectra show the two usual components: the quasi elastic component and the relaxed component. The Z distribution of the latter is fairly flat, slowly decreasing up to Z ≃ 15 and then rising again up to Z = 30. The variations in the Z distribution are more pronounced at the lower bombarding energy. The angular distributions associated with the relaxed component are forward

---

[†]On leave from DPhN/MF-CEN Saclay-France.

[*]On leave from Institut de Physique Nucléaire, Orsay, France.

[‡]Sloan Fellow 1974-76.

peaked for Z's close to that of the projectile and behave like $1/\sin\theta$ for larger Z's. The forward peaking is very substantial for $Z < 10$. For $Z > 10$ the forward peaking in excess of $1/\sin\theta$ disappears around $Z = 15$. These features are interpreted in terms of a diffusion process along the asymmetry coordinate of a short lived intermediate complex.

Nuclear reactions: $^{107,109}Ag + {}^{20}Ne$; $E_{^{20}Ne}$ = 175 MeV, 252 MeV. The atomic number of the emitted fragments has been determined up to Z = 32. The kinetic energy distribution, the cross section, and the angular distribution have been measured for each Z.

1) INTRODUCTION

In two previous studies on the reactions $^{14}N + {}^{107,109}Ag$ [1] and $^{40}Ar + {}^{107,109}Ag$, [2-4] evidence was discovered for the formation of a short-lived intermediate complex with well defined mass asymmetry (the shape corresponding perhaps to that of two touching spheres). This intermediate complex was characterized by the following properties: [5] i) The kinetic energy associated with the entrance channel appeared to be thermalized; ii) The forward peaking in the fragment angular distribution appeared to indicate a decay-time shorter than one mean rotational period, or about 10^{-21} sec; iii) The spread of the Z distribution of the fragments indicated that substantial particle exchange occurred during the life of the intermediate complex; iv) The changing angular distributions with the Z of the fragment, more sharply forward peaked for Z's close to that of the projectile, and approaching $1/\sin\theta$ for Z's farther away from

the projectile, suggested that the time evolution along the asymmetry coordinate is fairly slow, with a time constant comparable to the rotational period. The experimental data appeared to be consistent with a diffusion mechanism responsible for the particle exchange between the two fragments in contact. In fact a model based upon a diffusion equation, suggested by Moretto and Sventek,[6] seems to explain the main features of the experimental data.

The support to the diffusion theory comes from four physical observations: i) The low kinetic energies of the fragments; ii) The apparent sensitivity of the cross sections to V_z/T, where V_z is the potential energy of the intermediate complex (ridge potential energy) whose asymmetry is characterized by the Z of one of the two fragments, and T is the temperature of the intermediate complex; iii) The change in the mean time of emission of the fragments with Z as can be inferred from the change in forward peaking of the angular distributions with the difference between the Z of the fragment and the Z of the projectile; iv) The sensitivity of the cross sections and angular distributions upon the entrance channel mass asymmetry. Similar features are visible in many other experimental data obtained in a variety of heavy ion reactions.[1-14]

In the case of $^{40}Ar + ^{107,109}Ag$, the injection asymmetry is slightly to the right of the Businaro-Gallone maximum of the potential energy at the ridge,[5] on a gentle slope leading to the symmetric saddle point. The diffusion process seems to be responsible for the increasing cross section with increasing Z up to symmetric division and for a moderate forward peaking, somewhat more pronounced for fragments close in Z to the projectile. In the case of $^{14}N + ^{107,109}Ag$, the injection asymmetry is to the left of the

Businaro-Gallone maximum of the ridge potential energy, on a steep slope leading to extreme asymmetries. The diffusion process leads to a large cross section at low Z's, and to a very dramatic forward peaking for fragments with Z lower than that of the projectile, which heals rapidly for fragments with Z larger than that of the projectile.

The present combination of ^{20}Ne + $^{107,109}Ag$ is intermediate between the previous two cases. The injection asymmetry is close to the Businaro-Gallone maximum. To the left (lower Z's) there is a precipitous slope towards the extreme asymmetries, while to the right (higher Z's), the potential energy is almost flat, slowly sloping down towards the symmetric saddle point. Therefore an intermediate situation should be observed both in the Z distribution and in the angular distributions. It appears from the present results that this is indeed the case, thus providing more evidence for the diffusion mechanism mentioned above.

2) EXPERIMENTAL TECHNIQUE

The experiments were performed at the Berkeley 88 inch cyclotron using the $^{20}Ne^{6+}$ beam at 175 MeV and 252 MeV. Although obtained with a lower intensity, the Ne^{6+} 175 MeV beam was preferred to the Ne^{5+} 175 MeV beam in order to avoid a possible $^{12}C^{3+}$ or $^{16}O^{4+}$ contamination. The beam intensity was changed from angle to angle in order to maintain a reasonable counting rate. Approximately 100 nA of beam current were available on the target but near the grazing angle only a few nA were actually needed. The beam spot on the target was approximately 3 mm. in diameter.

The natural Ag targets, prepared by evaporation, were 300 $\mu g/cm^2$ thick. In the worst cases (target at 45° with respect to the beam direction and lower energy beam) the energy dispersion of the beam, introduced by the target, was close to 1.5 MeV which represents less than 1% of the nominal energy.

The products of the reaction were identified by means of two particle telescopes mounted on two independent arms rotating around the target center. Both telescopes were identical and were used simultaneously in order to increase the measurement efficiency. Each telescope was composed of a ΔE gas counter[15] and of an E solid state counter ($\sim$300 μm thick). The gas counter was an ionization chamber which gives a better resolution than the proportional counter used in previous experiments.[1,2,16] The ionization chamber was filled with a CH_4/Ar mixture (10% methane in volume). Later, for the 175 MeV experiment, the mixture was replaced by pure methane. With this gas a slightly better resolution was obtained. Furthermore a shorter rise time of the pulse allowed us to improve the timing between ΔE and E signals. The gas pressure inside the counters was stabilized by means of a cartesian manostat mounted down-stream from the chamber. The gas was pumped downstream and typically a 10 $cm^3 sec^{-1}$ gas flow was kept during the experiment. The pressures inside the counter were set in the range of 6.0 to 8.0 cm. of Hg corresponding to a thickness ranging from 0.368 to 0.491 mg/cm^2 of CH_4 at 20°C. A 50 $\mu g/cm^2$ plastic window (FORMVAR or VYNS), 3mm. in. diameter, was glued on the entrance frame of the counter in order to insulate the counter chamber, under pressure, from the scattering chamber under vacuum.

The entrance window of the counter was 6 cm. from the target center and the solid angle, defined by the window size, was typically 2 10^{-3} sr.

A schematic diagram of the electronic equipment is shown in fig.(1). The pulses coming from the two telescopes were fed to a standard linear and logic circuitry and were digitized by means of an analog multiplexer and ADC system. The digitized informations as well as the necessary identification markers were fed to the computer event by event. Then they were recorded on magnetic tape by blocks of 16 physical events. The data were analyzed off-line on a PDP9 computer and during the experiment two-dimensional ΔE-E maps were printed in order to check the performance of the experimental setup.

3) DATA REDUCTION

Z Identification

From the printed E-ΔE maps the different valleys separating one element from its neighbors could be identified. In order to reduce the amount of input data, each valley was approximated by a succession of straight lines. Without calibrating the ΔE and E pulses, there was always a way to identify the different products. In the data at forward angles, the Z of the projectile was quite obvious. At backward angles, at least two products could be identified without any ambiguity; carbon because its production cross section was always higher than those of its neighbors and fluorine for the opposite reason. This effect, which has been observed in Ar induced reactions on different targets,[2] can be explained by the peculiar proton binding energies of these two products as compared with those of their

neighbors. Only a few MeV of excitation energy are needed for a fluorine isotope to evaporate a proton and consequently to disappear as a fluorine. On the contrary the last proton is quite bound in a carbon isotope near β stability, so that proton evaporation is not very likely.

Energy calibration

The most accurate energy calibration has been obtained by means of elastic scattering. The energy deposited in the ΔE counter was computed from the Northcliff and Schilling tables and from the known composition and thickness of the gas inside the counter. The energy deposited in the solid state counter was obtained by difference, taking into account also the energy loss in the plastic window of the ΔE counter. It was assumed that there was no pulse height defect, which seems a reasonable assumption in the case of such a light particle, as Ne. All the charges created in the gas are not collected. More precisely, part of the charge created both close to the entrance and the exit sides of the counter is not gathered, due to the relative weakness of the electric field in these regions. We assumed that the charge which was not collected was a constant fraction of the collected charge. This might introduce an uncertainty of 5% in the absolute value of the measured ΔE energy for Z's far from that of the projectile. Furthermore the gas pressure was not directly measured inside the counter but slightly upstream, thus introducing a possible 3% additional uncertainty (difference between the pressures recorded with the counter by-pass open and closed). The relative uncertainty on the total kinetic energy due to the uncertainty in the calibration is not the same for all the products. For the higher Z's the energy deposited in the

ΔE counter may account for a large part of the total kinetic energy. Furthermore, due to the substantial center of mass velocity, the contribution of ΔE to the total energy is much more important in the backward than in the forward direction. Consequently one should be cautious in comparing the mean energies of the different products at various angles.

Dead layer energy corrections

Energy corrections were made both for the entrance window in the gas counter and for the target thickness. In the target, an average correction was made by assuming that the nuclear reactions take place in the middle layer of the target. The corrections have been made on the basis of the Nortcliff and Schilling tables. For each Z,the range energy curve was first fitted by a 5th degree polynomial expression and the energy loss was determined by interpolation. This energy correction is obviously most important for the higher Z's detected at low lab energy. In such cases the correction may account for 10% or even 20% of the measured energy. However, in most cases, the energy corrections are smaller than 5% of the measured values.

Lab. to c.m. transformation

The lab. to c.m. transformation was performed on the doubly differential cross section $\partial^2\sigma/\partial\Omega\partial E$ of the energy spectra. For each product, the corresponding $\theta_{c.m.}$, $E_{c.m.}$, and $(\partial^2\sigma/\partial\Omega\partial E)_{c.m.}$ were computed. Quantities such as the cross section integrated over energy:

$$\left.\frac{d\sigma}{d\Omega}\right|_{c.m.} = \int \left.\frac{\partial^2\sigma}{\partial\Omega\partial E_{c.m.}}\right|_{c.m.} dE_{c.m.} \; ;$$

the mean energy:

$$\bar{E}_{c.m.} = \left(\frac{d\sigma}{d\Omega}\Big|_{c.m.}\right)^{-1} \int E_{c.m.} \frac{\partial^2\sigma}{\partial\Omega\partial E_{c.m.}}\Big|_{c.m.} dE_{c.m.} \quad ;$$

the mean center of mass angle:

$$\bar{\theta}_{c.m.} = \left(\frac{d\sigma}{d\Omega}\Big|_{c.m.}\right)^{-1} \int \theta_{c.m.} \frac{\partial^2\sigma}{\partial\Omega\partial E_{c.m.}}\Big|_{c.m.} dE_{c.m.}$$

were also computed.

The distribution in $\theta_{c.m.}$ for a given $\theta_{lab.}$ due to the lab. kinetic energy distribution is quite narrow, except around 90°, where the FWHM for the $\theta_{c.m.}$ spectra is close to 5°. Obviously this dispersion tends to vanish in the forward and backward direction.

In the transformation from lab. to center of mass system, there is some uncertainty due to the fact that the masses of the fragments are not measured. Thus, for all the Z's, an arbitrary mass was chosen, equal to twice the atomic number. This assumption is probably quite good for the light fragments like C or O but is certainly less adequate for the highest Z's. In order to check the uncertainties introduced by this approximation, the other extreme assumption was made by assuming the neutron to proton ratio of the fragments to be the same as for the combined system.

In order to give an idea of the differences associated with the two approximations, let us consider the 252 MeV ^{20}Ne induced reactions and the product Z = 28 detected at $\theta_{lab.} = 20°$. The mean energy $\bar{E}_{c.m.}$ is found to be equal to 41.2 MeV with the first approximation, and 38.7 MeV with the second approximation. The center of mass cross sections are 506 mb and

522 mb respectively. Similarly for Z = 11, the largest Z observed at 156° lab. without low energy cut-off in the kinetic energy spectrum, the first approximation leads to $\overline{E}_{c.m.}$ = 49.5 MeV and the second one to $\overline{E}_{c.m.}$ = 51.3 MeV. The center of mass cross sections are 1090 mb and 1032 mb respectively. These two examples illustrate the uncertainty in the cross sections and in the mean energies introduced by the lack of knowledge of the masses.

Furthermore, as pointed out above, there is also some uncertainty in obtaining the center of mass cross section $d\sigma/d\Omega$ at a given $\theta_{c.m.}$, since the cross section measured at fixed $\theta_{lab.}$ corresponds to a finite distribution of center of mass angles. This uncertainty depends on the behavior of the angular distributions. If the angular distribution were isotropic in the center of mass, no correction would be needed. However, although this is actually not the case in the present reactions, the uncertainty remains quite small due to the rather symmetric shape of the energy spectra which tends to compensate for errors in the cross section. Thus, except for the cases where the cross section is varying very rapidly with θ, the assumption that $\sigma_{\overline{\theta}_{c.m.}} = \sigma_{\theta_{c.m.}}$ is satisfied within 2 or 3% error.

4) PRESENTATION OF THE RESULTS AND DISCUSSION

The kinetic energy distributions

Two components are observed in the kinetic energy distributions, similar in nature to those observed in other heavy ion reactions like $^{14}N + ^{107,109}Ag$ and $^{40}Ar + ^{107,109}Ag$.[1-4] The high energy component or quasi-elastic component is clearly visible for angles close to the grazing angle and for particles with atomic numbers close to that of the projectile.

In the examples plotted in Fig. (2) the quasi-elastic peak is visible for atomic numbers 7 through 12 at various laboratory angles. At the same time the "relaxed" peak is visible as a separate low-energy component which dominates for angles larger than the grazing angle. For low Z's, like Z = 6, the two components merge into a single broad peak and cannot be distinguished.

At larger angles, the "relaxed" peak dominates. The substantial similarity of the relaxed peaks at various angles, seen in other reactions, is also verified here. For a given Z, the center of mass "relaxed" kinetic energy distributions do not vary essentially with angle. Their nearly gaussian shape allows one to describe them in terms of their most probable values and their width. In Fig. (3) and Fig. (4) the most probable kinetic energies in the center of mass system are shown for various angles. It can be seen that these most probable energies do not change significantly with angle. The general trend with Z is, here as in other cases, consistent with the interpretation that the energies are arising essentially from Coulomb repulsion. The kinetic energies expected from the Coulomb repulsion of two touching spheres and of two touching spheroids allowed to attain their equilibrium deformation are also shown in Fig. (3). At large Z's it appears that the experimental kinetic energies are lower than the calculated Coulomb energies. This may mean that, for more symmetric configurations, the fragment deformation becomes larger with a consequent decrease in Coulomb repulsion. Also, the larger fragments are expected to lose more particles (neutrons and/or protons) by evaporation, thus reducing the fragment kinetic energy accordingly.

A comparison between the data at both bombarding energies shows that the most probable kinetic energies are somewhat larger at the larger bombarding energy. Similarly the widths (FWHM) are somewhat larger at the larger bombarding energy (Fig. 4). In conclusion, the overall features of the relaxed kinetic energy components are consistent with a nearly complete equilibration (relaxation) of the initial kinetic energy.[1,2,17] This, of course, is only a necessary but not sufficient condition to prove that a compound nucleus has been formed.

The Z Distribution

The laboratory cross sections at various angles as a function of Z are shown in Fig. (5) for both bombarding energies. The center of mass cross sections are shown in Fig. (7). The center of mass cross sections integrated over the experimental angular interval and extrapolated to a fixed angular interval are given in Table 1.

In the range $6 \leq Z \leq 15$ the cross sections are in general decreasing with increasing Z. At small angles the cross sections are very large and decrease rapidly. At larger angles the cross sections are smaller and do not decrease quite as rapidly. In the backward direction the cross sections are nearly constant with Z. For Z's larger than 16 the cross sections increase in a similar way with Z for all the angles. These general features are more evident in the 175 MeV than in the 252 MeV experiment. For instance the increase in cross section from $Z = 16$ to $Z = 28$ is approximately a factor of 3 to 4 at 175 MeV and barely a factor of two at 252 MeV bombarding energy. A strong even-odd effect favoring even Z's is also visible in the

TABLE 1. Integrated center of mass cross sections for individual atomic numbers. The first cross section column gives the cross section integrated over the experimental angular range $\theta_1 \div \theta_2$. The second cross section column gives the cross section interpreted from 30° to 130°. Due to the experimental errors and to the interpolation and extrapolation scheme used in evaluating the integrals, the quoted values may be in error by as much as 20%.

Z	θ_1	θ_2	$2\pi\int_{\theta_1}^{\theta_2} \frac{d\sigma}{d\Omega} \sin\theta d\theta$	$2\pi\int_{30°}^{130°} \frac{d\sigma}{d\Omega} \sin\theta d\theta$	θ_1	θ_2	$2\pi\int_{\theta_1}^{\theta_2} \frac{d\sigma}{d\Omega} \sin\theta d\theta$	$2\pi\int_{30°}^{130°} \frac{d\sigma}{d\Omega} \sin\theta d\theta$
	deg	deg	mb	mb	deg	deg	mb	mb
	E = 175 MeV				E = 252 MeV			
5	71.96	160.91	2.17	6.11	106.94	161.91	2.73	10.39
6	62.96	161.91	8.76	24.06	37.98	161.91	33.03	40.07
7	61.96	161.91	3.63	10.07	39.98	161.91	13.52	17.35
8	62.96	161.91	4.49	11.74	39.98	163.91	12.48	15.20
9	50.97	163.91	3.14	6.12	38.98	161.91	6.29	7.34
11	36.98	161.91	4.73	5.10	24.98	136.93	7.95	6.78
12	26.98	152.92	7.46	6.09	25.98	138.92	7.84	6.88
13	26.98	118.93	3.89	4.01	27.98	125.93	5.63	5.65
14	26.98	118.93	3.94	4.23	29.98	112.94	5.08	5.99
15	31.98	121.93	2.60	2.93	26.98	112.94	4.10	4.70
16	28.98	120.93	3.22	3.54	27.98	114.94	4.21	4.83
17	27.98	120.93	2.67	2.92	29.98	113.94	4.14	5.01
18	22.98	119.93	3.45	3.60	29.98	114.94	4.49	5.33
19	21.98	101.94	3.17	4.34	30.98	115.94	4.74	5.60
20	22.98	101.94	3.51	4.94	28.98	101.94	4.35	6.13
21	21.98	81.95	3.13	4.93	28.98	97.95	4.62	8.33
22	22.98	82.95	3.60	6.21	29.98	96.95	5.01	8.33
23	21.98	84.95	4.11	6.87	29.98	87.95	4.13	7.16
24	21.98	84.95	4.53	6.51	30.98	88.95	4.29	7.78

cross sections, especially at low Z's. These fluctuations, similar in amplitude at both energies, may possibly be due to secondary evaporation from the fragments.

It appears that the general trends observed in the Z distributions can be easily related to the potential energy of the ridge line. The ridge line is the locus of saddle points constrained to a fixed mass asymmetry. An example of ridge lines for various angular momenta is shown in Fig. (6). In general, assuming that either a compound nucleus is formed, or that the system is formed directly at the ridge and undergoes equilibration along the asymmetry mode, the following expression should give a good representation of the particle yield:

$$Y(Z) \propto \exp(-V_Z/T)$$

where the Z of one of the two fragments has been used to describe the asymmetry at the ridge; V_Z is the potential energy at the ridge; and T is the ridge temperature. A log plot of the cross sections or yields versus Z should reflect a linear dependence with V_Z/T. A cursory inspection of the experimental data show that this is approximately the case. The high cross sections for low Z's reflect the low potential energy at the ridge in this region. Also, the increase in cross section for higher Z's, towards the symmetric splitting, is consistent with the theoretical slight depression in the ridge potential energy close to symmetry, especially visible at large ℓ values. Furthermore, the fact that these features are more strongly visible at low energy is a possible illustration of the 1/T effect.

However, it is not at all obvious that a complete equilibration has occurred along the mass asymmetry mode. A comparison with other heavy ion reactions leading to similar combined systems, while not conclusive, is very suggestive of incomplete equilibration.[5] In the reaction $^{107,109}Ag + {}^{14}N$,[1] there is a great enhancement of low Z products as compared with the present reactions without any strong indication of an increasing cross section with increasing Z for $Z > 16$. On the other hand, in the reaction $^{107,109}Ag + {}^{40}Ar$,[2] the cross sections dramatically increase with increasing Z from $Z > 9$, without any obvious increase of the cross section for lower Z's. In other words, the present reaction appears to be intermediate in its features between the two reactions mentioned above. One can possibly argue that the observed effect is exclusively related to the gradual increase of the fissility parameter x from the system $^{107,109}Ag + {}^{14}N$ to the system $^{107,109}Ag + {}^{40}Ar$. In fact, as one moves towards x values above the Businaro-Gallone point, a minimum develops in the potential energy mode along the mass asymmetry. Yet the systems are so close to one another, that a more likely cause for the observed features in the three reactions may be the initial target-projectile asymmetry.[5]

This is consistent with the hypothesis, formulated by Moretto and Sventek,[6] that an intermediate complex of definite mass asymmetry (having a shape close to that of two touching fragments) and completely thermalized in kinetic energy, diffuses along the mass asymmetry coordinate while rotating and decaying. This hypothesis explains on the one hand the gross V_z/T dependence of the particle yields, and on the other hand it explains the large enhancement of low Z particles in N + Ag, of larger Z particles in Ar + Ag and the intermediate situation for Ne + Ag. In

the first case the injection asymmetry is to the *left* of the potential energy maximum (Fig. 6), leading to a diffusion towards small Z's; in the second case the injection point is to the *right* of the potential energy maximum, leading to a diffusion towards large Z's; in the present case, the injection asymmetry is approximately on top of the potential energy maximum, thus generating the observed intermediate features. A very strong argument in favor of the existence of an intermediate complex and of diffusion along the asymmetry coordinate is provided by the angular distribution.

The angular distributions

The center of mass angular distributions associated with the various Z's are shown in Fig. (7) for the two bombarding energies. Care has been taken to either subtract any cross section associated with identifiable quasi-elastic components of the kinetic energy if any, or to eliminate the point altogether from the plot if the subtraction proved to be either uncertain or impossible. No contamination of quasi-elastic cross section larger than 3%, should be present in the plotted angular distribution.

The general features of the angular distributions can be summarized as follows. For $Z < 10$ a strong forward peaking is observed, well above $1/\sin\theta$; the minimum, instead of being at 90° is displaced backwards at ~120°; a distinct but much less pronounced rise is observed in the backward direction. For $Z > 10$ the strong forward peaking becomes progressively more gentle, until, around $Z = 15$ and above, the angular distributions become indistinguishable from $1/\sin\theta$. At the same time the minimum gradually moves forward from ~120° to 90°.

A strong energy dependence is also observed in the angular distributions. In all cases the forward peaking is substantially more pronounced at the lower bombarding energy. Similarly, the minimum is slightly farther in the backward hemisphere, at times by as much as 10°, at low bombarding energy than at high bombarding energy. Yet the forward peaking appears to die off just as fast at both energies as one moves from $Z = 10$ to $Z = 15$ and above. This overall behavior appears to be consistent with the hypothesis of an intermediate complex diffusing along the asymmetry mode while rotating and decaying.

The usual conclusions can be drawn about the decay and the kinetic energy dissipation.[1,2] They clearly occur on a time scale much shorter than the mean rotational period. This can be simply inferred from the forward peaking. On the other hand, the diffusion along the asymmetry coordinate appears to proceed at a much slower rate. The strong forward peaking observed at $Z < 10$ can be explained by noticing that the injection asymmetry places the system either at the top or to the left of the potential energy peak. A rapid diffusion to the left is expected which populates the low Z's quite rapidly and which allows them to decay also quite rapidly (hence the strong forward peaking). The rapidly vanishing forward peaking for $Z > 10$ can be understood in terms of a slow diffusion to the right which, depending upon the ℓ wave, is either uphill or occurring on a fairly flat potential energy region.

A fairly consistent picture can be obtained by comparing the present case with the $^{14}N + ^{107,109}Ag$ and with the $^{40}Ar + ^{107,109}Ag$. In the former case, one has strong forward peaking for $Z < 7$ and a rapidly decaying forward

peaking for $Z > 7$ until a $1/\sin\theta$ distribution is observed around and above $Z = 13$. This is consistent with an injection asymmetry to the *left* of the potential energy peak. In the latter case one observes only a moderate forward peaking below $Z = 18$ which is decreasing for lower Z's. This is consistent with an injection asymmetry slightly to the right of the potential energy peak.

It is not clear what to conclude about the very high Z's, between say, 20 and 30. While the diffusion model proposed by Moretto and Sventek[6] can indeed predict $1/\sin\theta$ angular distributions without assuming compound nucleus formation, it is not possible to conclude to what extent a compound nucleus is involved in the emission of these products. Only a quantitative calculation, now in progress, consistently fitting all the available data for the various reactions can give the answer.

5) SUMMARY AND CONCLUSIONS

The present study of the reaction of $^{20}Ne + ^{107,109}Ag$ has revealed on the one hand gross similarities with previously studied reactions, and on the other has shown tantalizing differences.

The kinetic energy spectra are characterized by the two typical components: quasi-elastic and relaxed. The latter component, as in previous reactions, indicates a nearly complete equilibration of the kinetic energy.

The cross section of the relaxed component, as a function of the Z of one of the fragments shows two interesting features. The first is an

indication that the cross section depends upon the ratio V_z/T. The second is the shape of the charge distribution, intermediate between those obtained in two previously studied reactions, $^{14}N + ^{107,109}Ag$ and $^{40}Ar + ^{107,109}Ag$. This seems to indicate that the system remembers the entrance channel asymmetry and that the final distribution in asymmetries (observed charge distribution) has been originated through a diffusive time evolution.

Further evidence of this diffusion mechanism is found in the angular distribution for the various atomic numbers. Large forward peaking, in excess of $1/\sin\theta$ is visible for particles close in Z to the projectile. The decrease in forward peaking for particles farther removed from the projectile is interpreted in terms of the increased time lag between initial interaction and decay, due to the longer time necessary to populate Z's farther removed from the projectile. The stronger forward peaking visible for $Z < Z_{proj}$ and the rapid symmetrization of the angular distribution for $Z > Z_{proj}$ is taken as an effect of the potential energy of the intermediate complex upon the rate of diffusion.

ACKNOWLEDGMENTS

The authors wish to thank the 88" Cyclotron staff for their help and assistance.

References

1. L. G. Moretto, S. K. Kataria, R. C. Jared, R. Schmitt and S. G. Thompson, Lawrence Berkeley Report LBL-4063, May 1975.
2. J. Galin, L. G. Moretto, R. Babinet, R. Schmitt, R. Jared and S. G. Thompson, Lawrence Berkeley Report LBL-4064, June 1975.
3. L. G. Moretto, D. Heunemann, R. C. Jared, R. C. Gatti and S. G. Thompson, Physics and Chemistry of Fission 1973, International Atomic Energy Agency, Vienna, 1974 V. II, p. 351.
4. S. G. Thompson, L. G. Moretto, R. C. Jared, R. P. Babinet, J. Galin, M. M. Fowler, R. C. Gatti and J. B. Hunter, Nobel Symposium on Superheavy Elements, (1974). Physica Scripta Vol. 10-A.
5. L. G. Moretto, R. P. Babinet, J. Galin and S. G. Thompson, Lawrence Berkeley Laboratory Report LBL-3444, November 1974, to be published in Physics Lett.
6. L. G. Moretto and J. S. Sventeck, Lawrence Berkeley Laboratory Report LBL-3443, November 1974, to be published in Physics Lett.
7. J. Galin, D. Guerreau, M. Lefort, J. Péter and X. Tarrago, Nucl. Phys. A 159 (1970) 461.
8. A. G. Artukh, V. V. Avdeichikov, G. F. Gridnev, V. L. Mikheev, V. V. Volkov and J. Wilczinski, Nucl. Phys. A167 (1971) 284.
9. A. G. Artukh, G. F. Gridnev, V. L. Mikheev, V. V. Volkov and J. Wilczinski, Nucl. Phys. A211 (1973) 299.
10. A. G. Artukh, G. F. Gridnev, V. L. Mikheev, V. V. Volkov and J. Wilczinski, Nucl. Phys. A215 (1973) 91.

11. F. Hanappe, C. Ngô, J. Péter, B. Tamain, Physics and Chemistry of Fission 1973 International Atomic Energy Agency Vienna, 1974 V. II, p. 289.

12. F. Hanappe, M. Lefort, C. Ngô, J. Péter and B. Tamain, Phys. Rev. Lett. 32 (1974) 738.

13. K. L. Wolf, J. P. Unik, J. R. Huizenga, V. E. Viola, J. Birkelund and H. Freiseleben, Phys. Rev. Lett. 33 (1974) 1105.

14. For a complete list of references see A. Fleury and J. M. Alexander, Ann. Rev. Nucl. Sci. 1632-4 (1974) 279.

15. M. M. Fowler and R. C. Jared, Nucl. Inst. Meth. 124 (1975) 341.

16. K. D. Hildenbrand, H. H. Gutbrod, W. V. Oertzen and R. Bock, Nucl. Phys. A157 (1970) 297.

17. L. G. Moretto, Lawrence Berkeley Laboratory Report LBL-3454, Jan 1975, to be published in Nucl. Phys.

FIGURE CAPTIONS

Fig. 1. Schematic diagram of the electronic equipment.

Fig. 2. Examples of the center-of-mass kinetic energy distributions for fragments with atomic numbers close to that of the projectile at various laboratory angles. Notice how the quasi elastic component vanishes at large angles. Fragments with larger and smaller Z's are characterized by Gaussian kinetic energy distributions.

Fig. 3. Average center of mass kinetic energies as a function of Z for various laboratory angles. The two lines are the calculated fragment energies arising from Coulomb repulsion for two spheres in contact and two spheroids in contact at equilibrium deformation.

Fig. 4. Average center-of-mass kinetic energies and widths (FWHM) for various Z's as a function of c.m. angle. The widths are indicated by means of error bars. Notice the slight decrease in mean energy and in width with increasing angle, for Z's close to 10.

Fig. 5. Laboratory cross sections $\left.\frac{d\sigma}{d\Omega}\right|_{lab}$ as a function of Z at various laboratory angles.

Fig. 6. Potential energies of three different intermediate complexes as a function of the Z of one of the fragments for various ℓ waves. The arrows indicate the injection asymmetries associated with the reactions quoted in the figure.

Fig. 7. Center-of-mass angular distributions for the various fragments. The lines passing through the data for Z>15 correspond to $W(\theta) \propto 1/\sin\theta$.

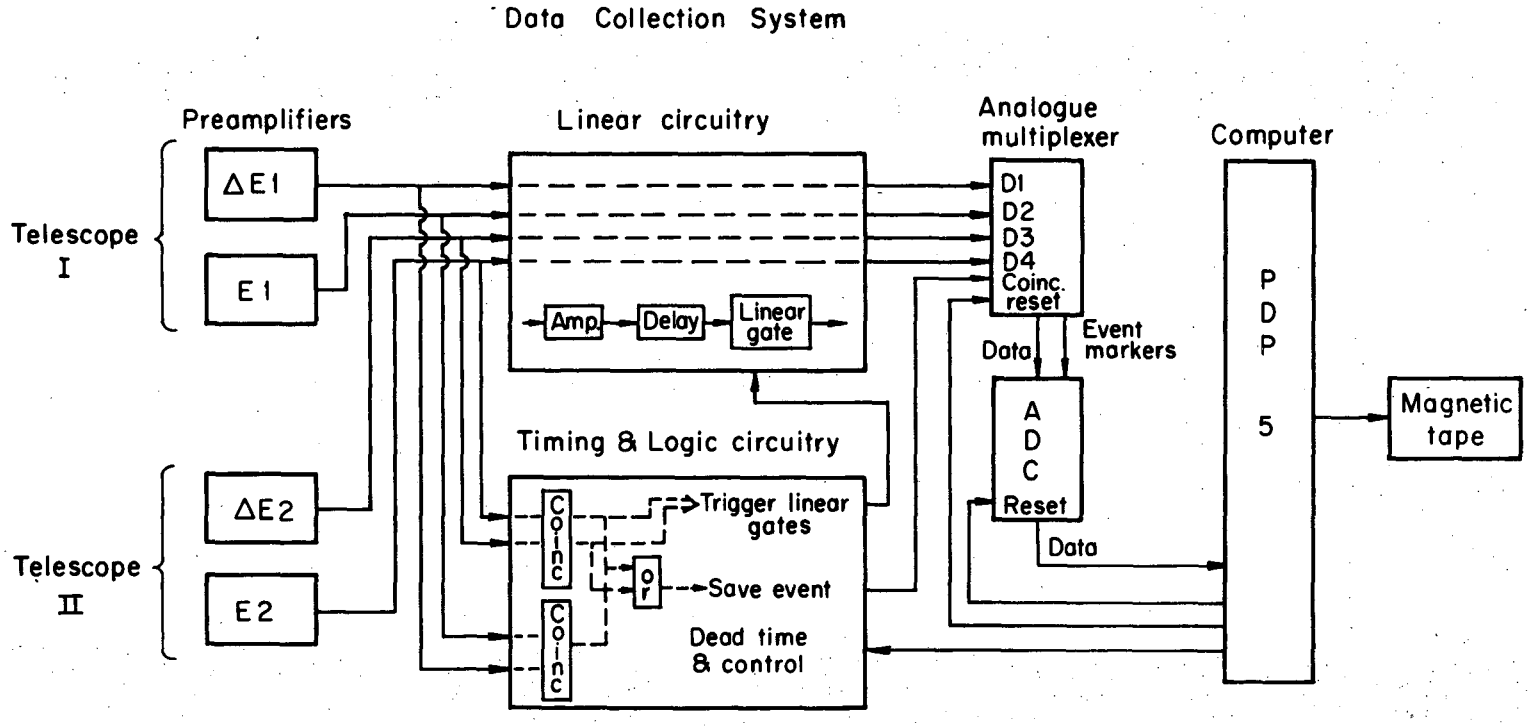
Data Collection System
Preamplifiers
Linear circuitry
Analogue multiplexer
Computer
Telescope I
ΔE1
E1
Amp
Delay
Linear gate
D1
D2
D3
D4
Coinc. reset
Event markers
Data
P
D
P
5
Magnetic tape
A
D
C
Reset
Data
Timing & Logic circuitry
Telescope II
ΔE2
E2
Coinc
Coinc
Trigger linear gates
or
Save event
Dead time & control
XBL737-3334A

Fig. 1

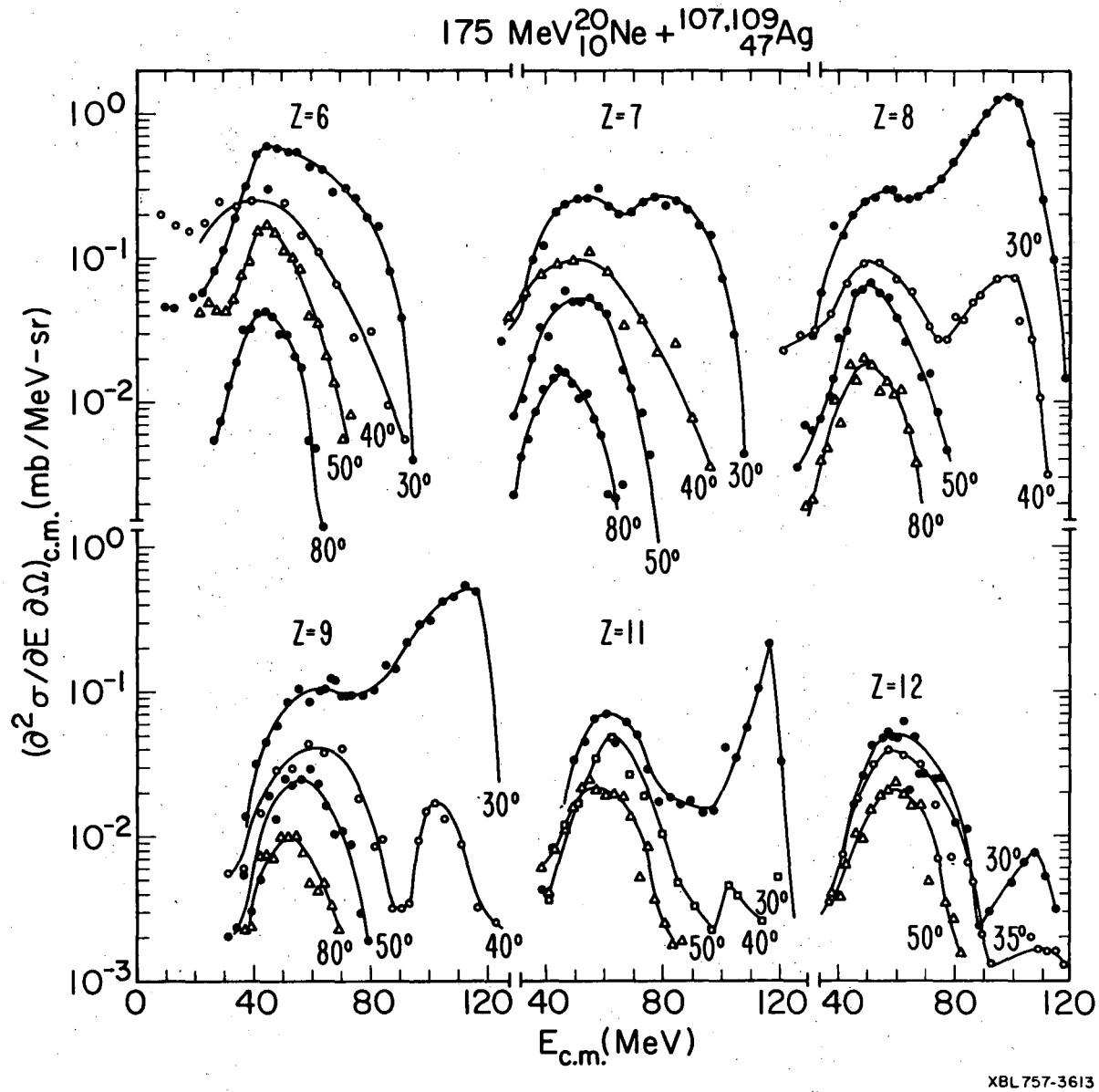

Fig. 2a

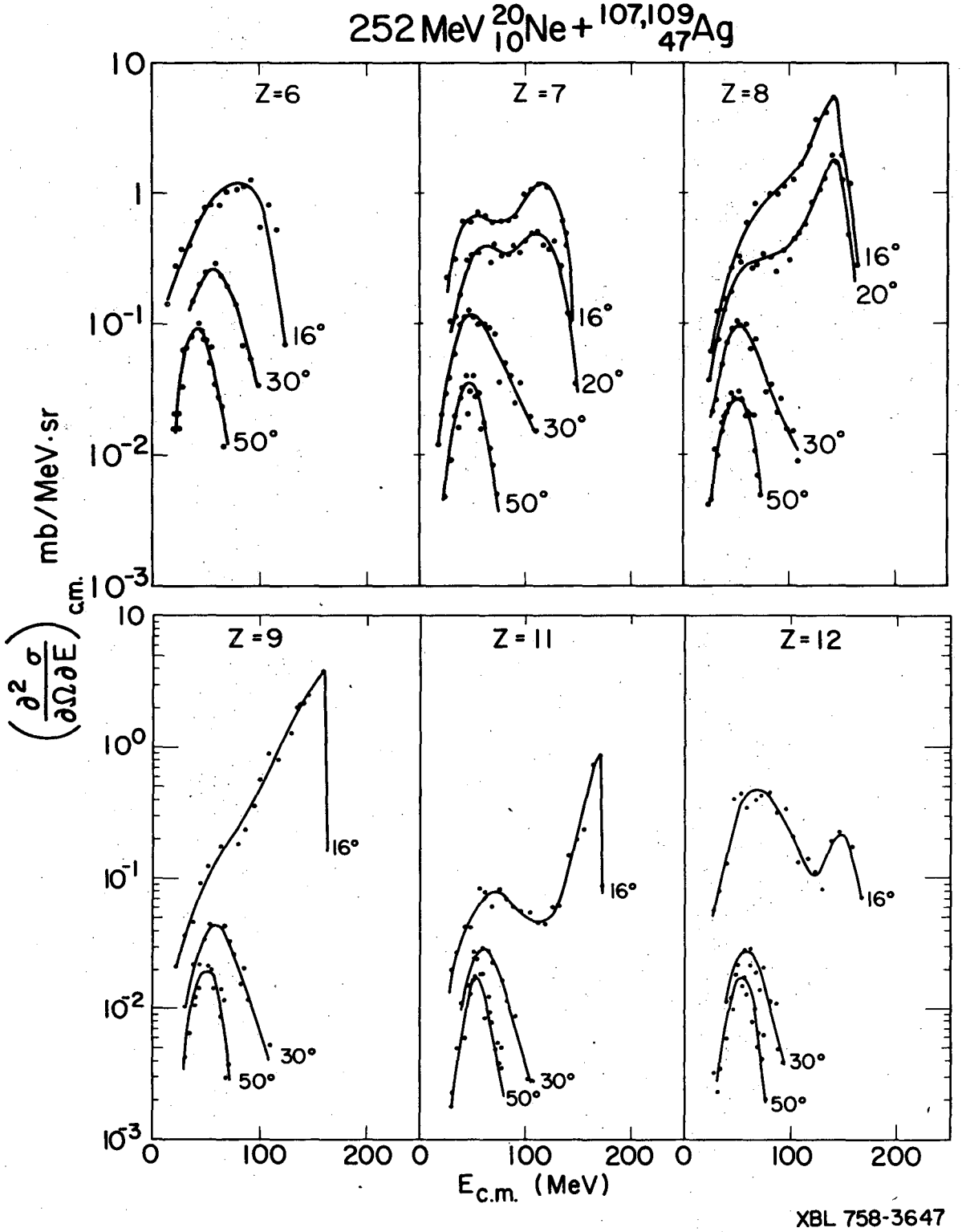
252 MeV $^{20}_{10}$Ne + $^{107,109}_{47}$Ag
Z=6
Z=7
Z=8
Z=9
Z=11
Z=12
16°
20°
30°
50°
mb/MeV·sr
$\left(\frac{\partial^2\sigma}{\partial\Omega\partial E}\right)_{c.m.}$
$E_{c.m.}$ (MeV)
XBL 758-3647

Fig. 2b

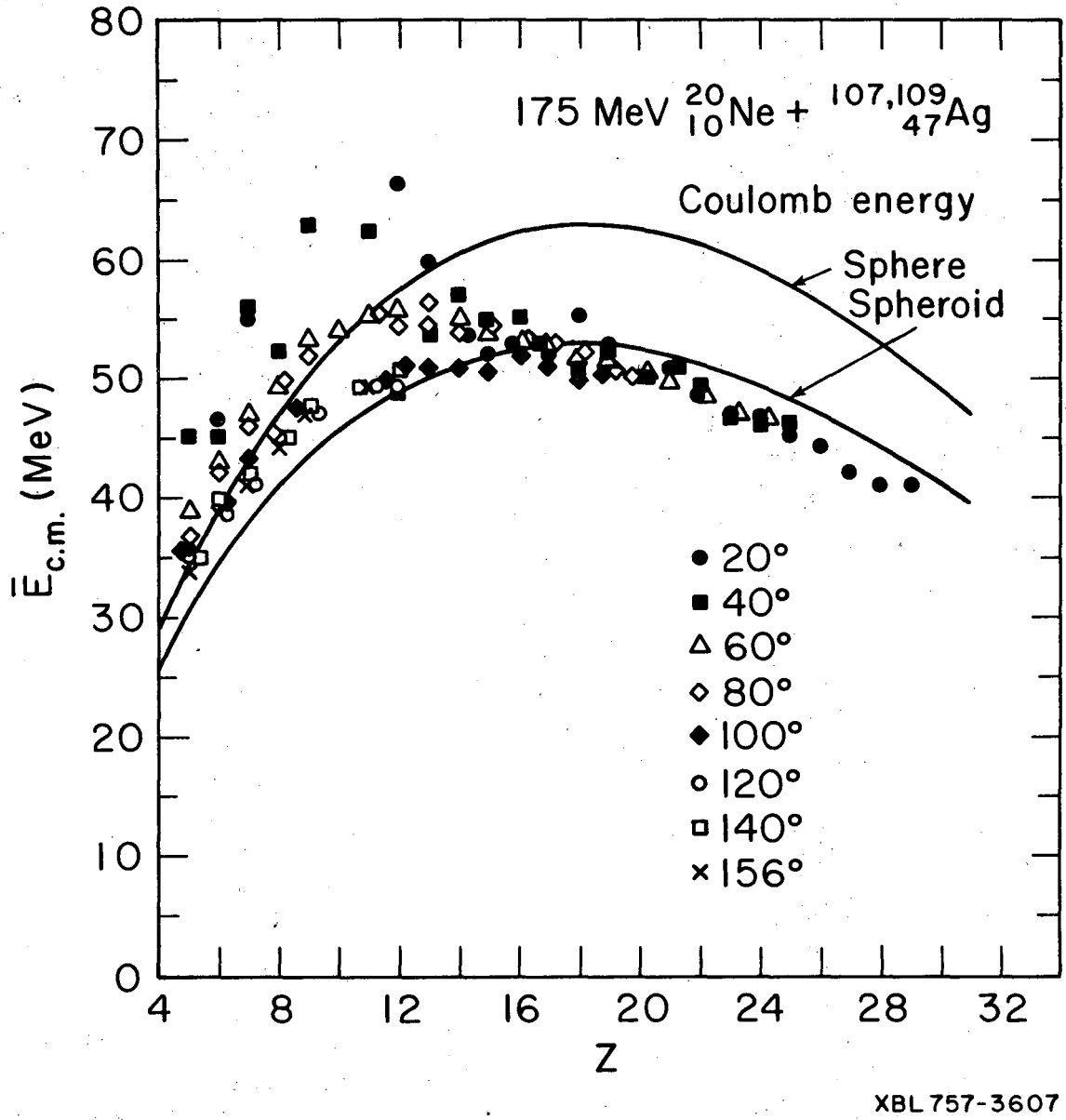

Fig. 3a

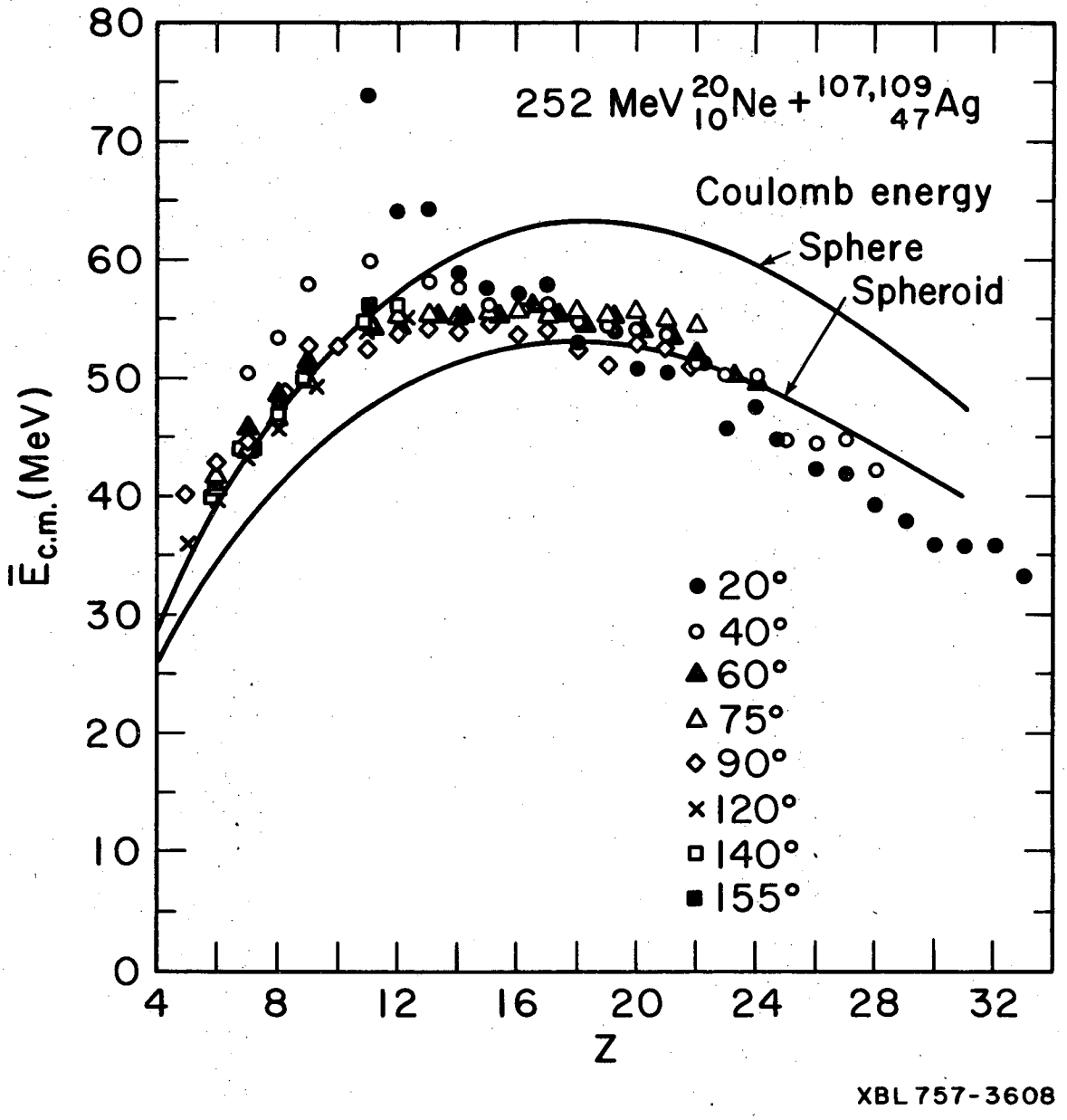
252 MeV $^{20}_{10}$Ne + $^{107,109}_{47}$Ag
Coulomb energy
Sphere
Spheroid
20°
40°
60°
75°
90°
120°
140°
155°
$\bar{E}_{c.m.}$ (MeV)
Z
0
10
20
30
40
50
60
70
80
4
8
12
16
20
24
28
32
XBL 757-3608

Fig. 3b

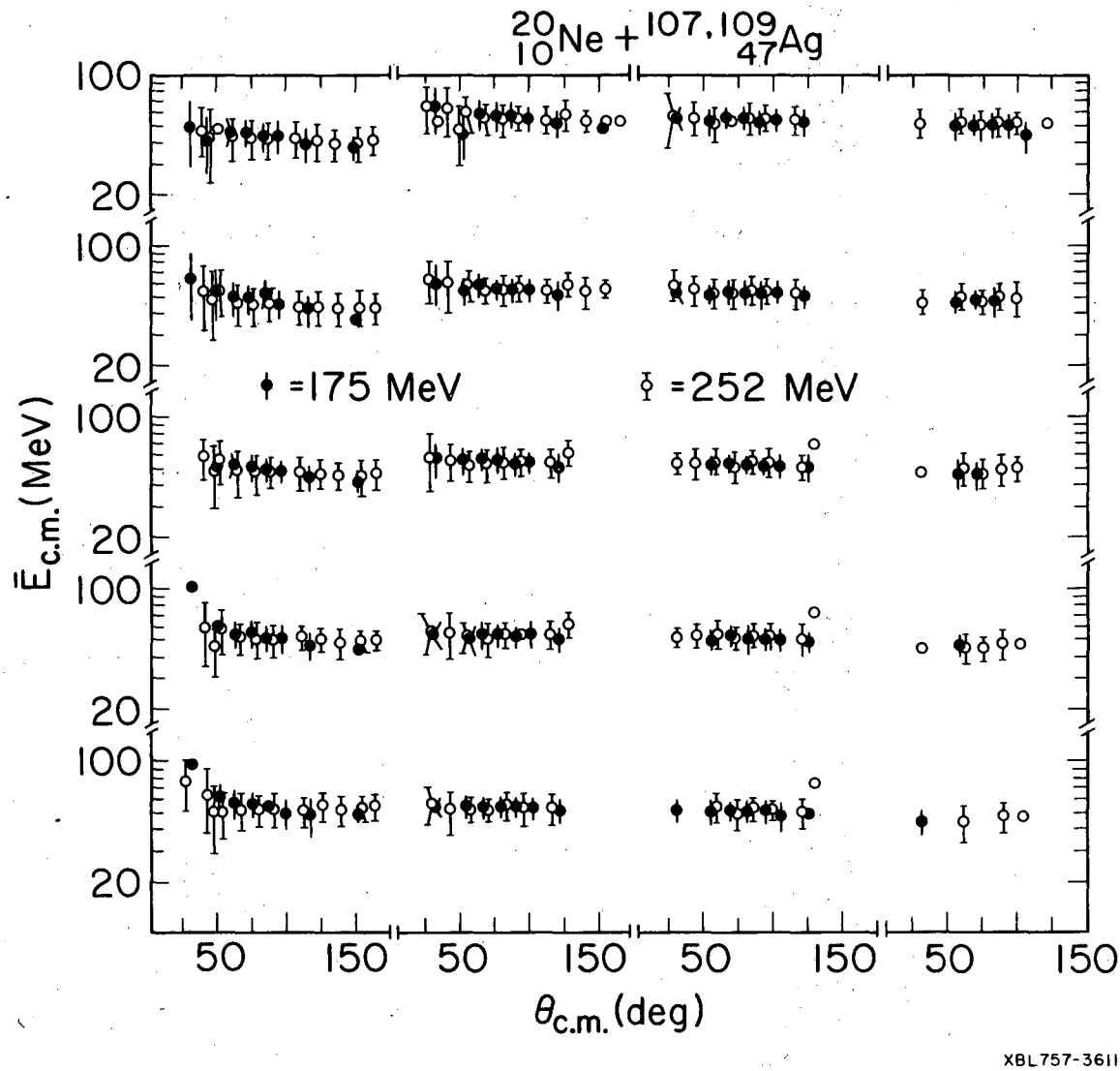

Fig. 4

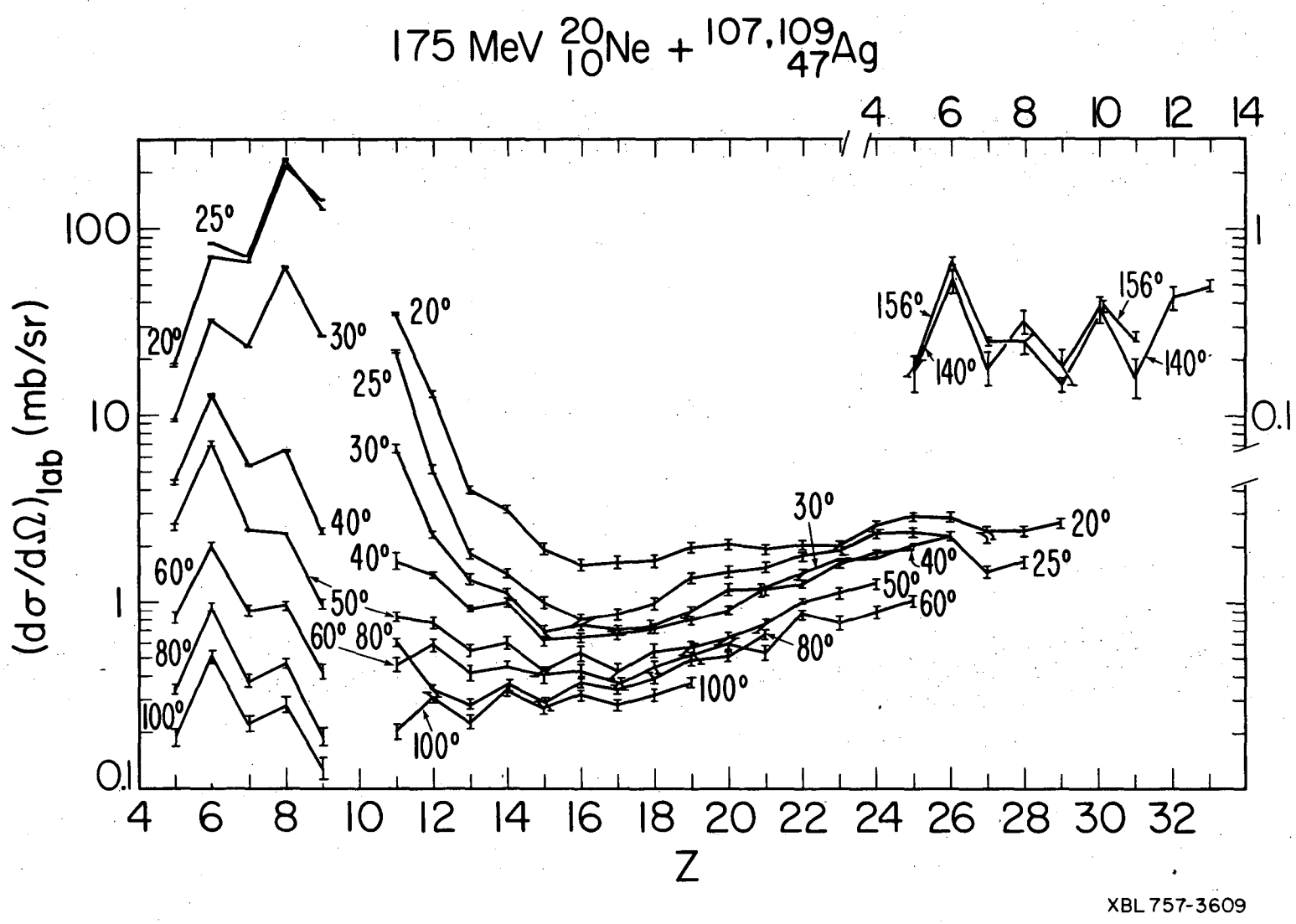
175 MeV $^{20}_{10}$Ne + $^{107,109}_{47}$Ag
$(d\sigma/d\Omega)_{lab}$ (mb/sr)
Z
25°
20°
30°
40°
60°
50°
80°
100°
156°
140°
XBL 757-3609

Fig. 5a

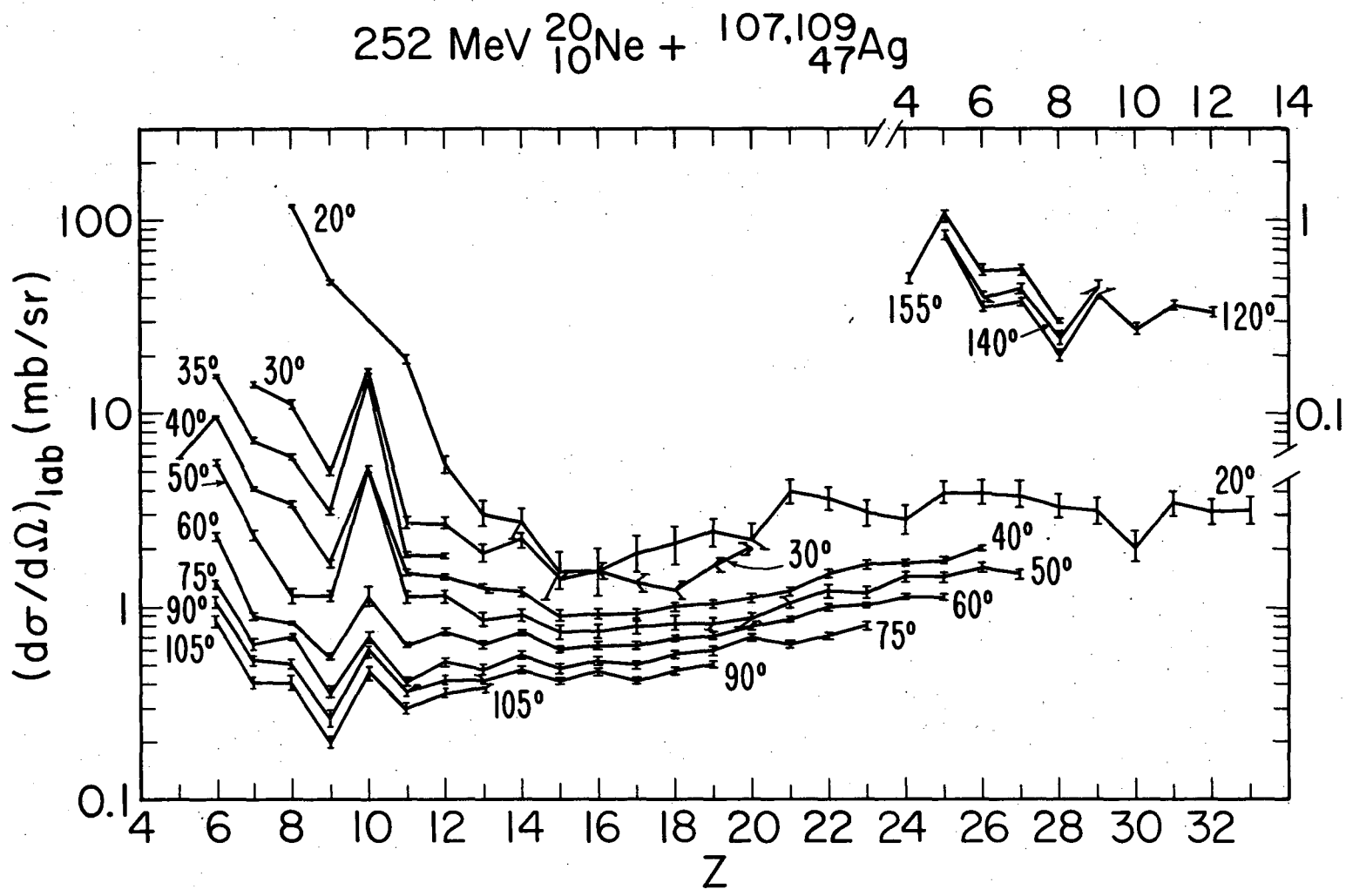

Fig. 5b

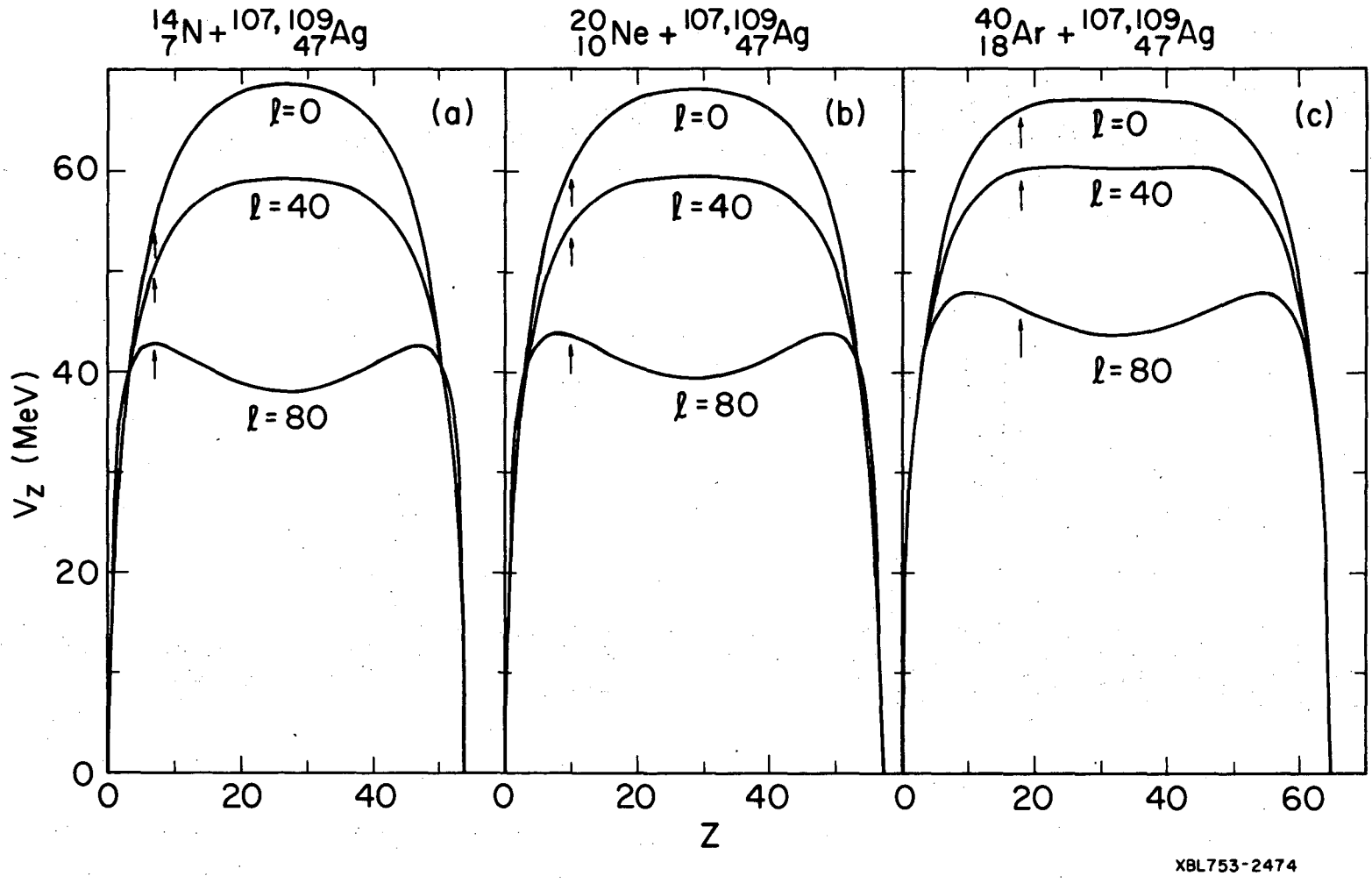
$^{14}_{7}N + ^{107,109}_{47}Ag$
$^{20}_{10}Ne + ^{107,109}_{47}Ag$
$^{40}_{18}Ar + ^{107,109}_{47}Ag$
(a)
(b)
(c)
ℓ=0
ℓ=40
ℓ=80
V_Z (MeV)
Z
0
20
40
60
XBL753-2474

Fig. 6

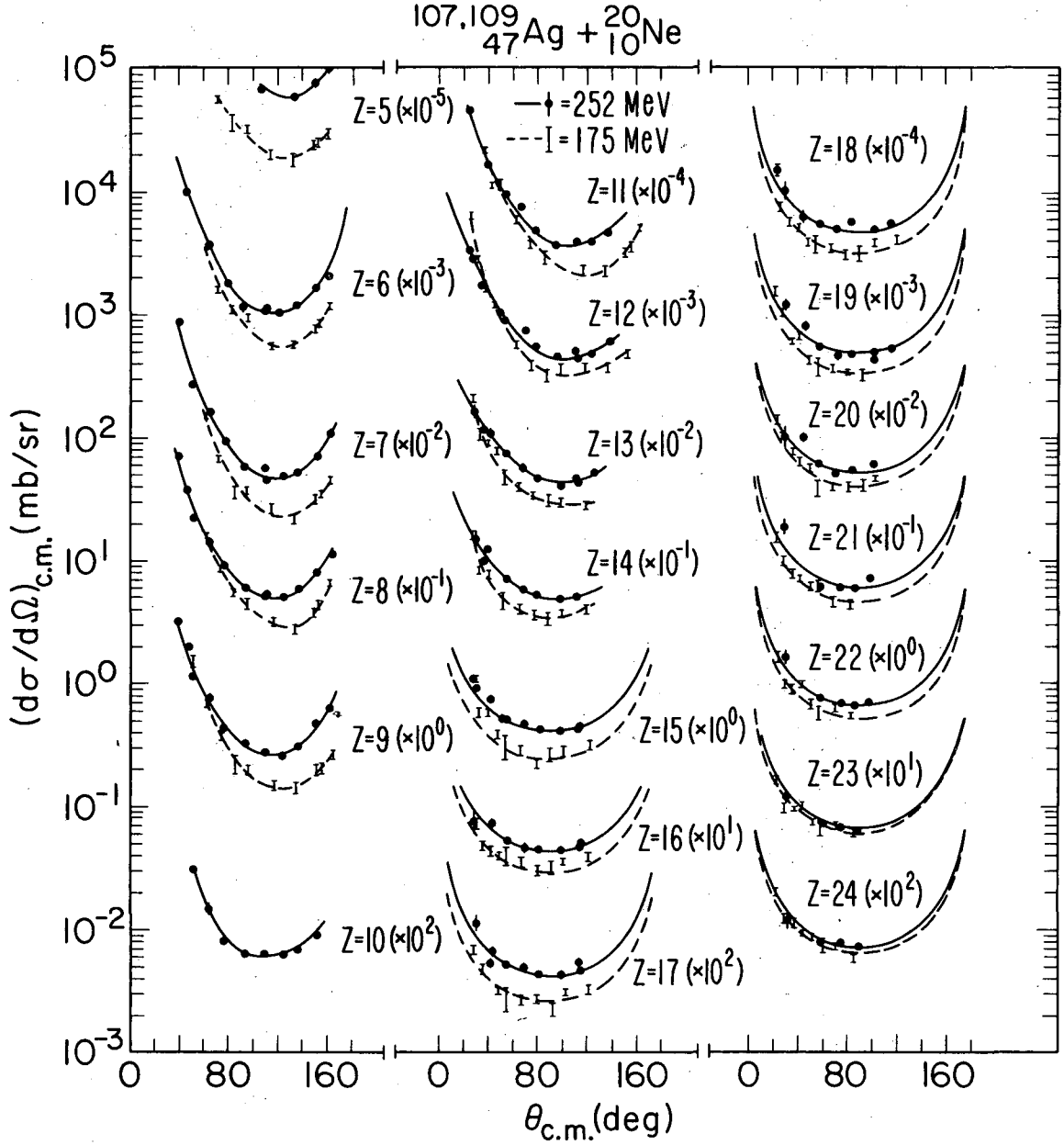

Fig. 7

TECHNICAL INFORMATION DIVISION
LAWRENCE BERKELEY LABORATORY
UNIVERSITY OF CALIFORNIA
BERKELEY, CALIFORNIA 94720